Extremely Small Iron Oxide Nanoparticles with pH-Dependent Solubility Transition as T 1 /T 2 Switchable Contrast Agents for MRI

Yilin He, Zheng Mao, Zhongzhong Lu, Jincong Yan, Ye Zhang, Alberto Bianco, Yi Cao, Renjun Pei

Extremely Small Iron Oxide Nanoparticles with pH-Dependent Solubility Transition as T_1/T_2 Switchable Contrast Agents for MRI

Yilin He[1,2], Zheng Mao[1], Zhongzhong Lu[1], Jincong Yan[1], Ye Zhang[1], Alberto Bianco[2], Yi Cao[,1], Renjun Pei[*,1]*

[1] Suzhou Key Laboratory of Functional Molecular Imaging Technology, CAS Key Laboratory of Nano-Bio Interface, Division of Nanobiomedicine, Suzhou Institute of Nano-Tech and Nano-Bionics, Chinese Academy of Sciences, Suzhou 215123, China

[2] CNRS, Immunology, Immunopathology and Therapeutic Chemistry, UPR 3572, University of Strasbourg, ISIS, 67000 Strasbourg, France

[*]Corresponding Authors:

Renjun Pei, E-mail: rjpei2011@sinano.ac.cn; Tel.: +86 0512 65822776

Yi Cao, E-mail: ycao2014@sinano.ac.cn; Tel.: +86 0512 62872587

ABSTRACT: Extremely small iron oxide nanoparticles (ESIONPs) with a switchable contrast signal and a favorable biocompatibility are gaining considerable attention as smart magnetic resonance imaging (MRI) contrast agents (CAs). To improve the accuracy of tumor diagnosis using adaptive MRI CAs, that realize rapid imaging signal conversion under an endogenous stimulus, are highly demanded. Herein, based on the hydrophilic to hydrophobic transition of polymers, we propose a pH-responsive T_1/T_2 switchable ESIONP contrast agent. ESIONPs are functionalized at the surface with

adamantane groups through a polyethylene glycol (PEG) chain, and subsequently a stimuli-responsive polymer (PSDM) with pH-dependent solubility is introduced through the host-guest interaction between adamantane and β-cyclodextrin (β-CD). The obtained ESIONPs-PEG-PSDM is equipped with the remarkable pH responsiveness, which triggers the aggregation of ESIONPs under the tumor acid condition, leading to the switch from a T_1 to a T_2 contrast agent. *In vivo* MRI experiments show that T_2 contrast signal is selectively enhanced at the tumor location after injection of ESIONPs-PEG-PSDM. Therefore, ESIONPs-PEG-PSDM with pH-induced hydrophilic to hydrophobic transition is a potential smart MRI contrast agent for the precise tumor diagnosis.

KEYWORDS: host-guest interaction, relaxivity, biocompatibility, tumor microenvironment, tumor diagnosis

1. INTRODUCTION

MRI is an established clinical imaging technique for the tumor diagnosis with noninvasive and nonionizing radiative property as well as high temporal and spatial resolution.[1-3] In the clinic, exogenous contrast agents that can shorten the relaxation time of water protons have been introduced to overcome the intrinsic limited sensitivity of MRI.[4-5] Those molecules that primarily reduce the longitudinal relaxation time (T_1) are normally identified as T_1 CAs and can provide positive contrast enhancement, represented by gadolinium-based small molecules. While those agents that mostly affect the transverse relaxation time (T_2) are generally considered as T_2 CAs and can provide negative contrast enhancement, represented by superparamagnetic iron oxide nanoparticles (SPIONs).[6] Although these traditional T_1 and T_2 CAs are able to improve the contrast effectiveness, their "always on" contrast signals usually lead to a lack of specificity and generate a high background signal, which may disturb the precision and efficiency of clinical tumor diagnosis.[7-9] Hence, stimulus-responsive CAs, whose signal can be amplified or activated in response to the stimuli derived from the tumor microenvironment, have drawn great attention in recent years.[1, 10] Towards the development of stimulus-responsive CAs, several strategies have been explored to specially enhance T_1 or T_2 MRI signal.[11-13] For instance, pH-responsive gadolinium nanoparticle functionalized with gadolinium triacetate and silkworm sericin was designed to improve T_1 relaxivity in vivo.[14] However, these stimulus-responsive CAs with the performance of single T_1 or T_2 signal amplification cannot still completely avoid the background signal in the inactive state, which brings a negative impact on the

precise diagnosis.[15-16] Therefore, an efficient method of switching contrast effect between T_1 and T_2 at the special pathological microenvironment that can fundamentally improve the signal-to-noise ratio may be considered a promising approach.

ESIONPs with a diameter less than 4 nm were found to have the ability of enhancing T_1 MRI contrast and regarded as an interesting type of T_1 CAs.[8, 17-18] The unique property of ESIONPs is ascribed to the unpaired electrons of Fe^{3+} on the large surface area and the small magnetic moment resulted from the extremely small size of the particles.[19] Recently, research studies have pointed out that the magnetic field inhomogeneity of aggregated ESIONPs could significantly increase due to the magnetic coupling, thus providing T_2 MRI contrast effect.[16, 20] The type of contrast enhancement of ESIONPs can be regulated by the transition between a dispersed and an aggregated condition, which may provide a feasible method for the design of stimulus-responsive T_1-T_2 switchable CAs, converting the contrast effect between T_1 and T_2.

Several efforts have been made to construct T_1-T_2 switchable CAs by triggering the assembly or disassembly of ESIONPs at the tumor location.[15, 17, 21-24] For instance, ultrasmall Fe_3O_4 NPs have been synthesized and cross-linked using cystamine, and the resulting nanoclusters can dissociate to single particles under tumor microenvironment switching from T_2 to T_1 behavior.[25] For T_2/T_1 switchable CAs designed by the conversion from aggregated to dispersed state in the pathological region, the dispersed ESIONPs with extremely small size will easily present the intravasation back into circulation to some extent. As a result, this type of design will lead to the adverse effect on the accumulation effect of CAs at the tumor region.[26] For T_1/T_2 switchable CAs

based on ESIONPs, the small sized NPs are more efficient to extravasate from the leaky tumor vessel and permeate further into the tumor. After their aggregation at the pathological region, the clustered NPs are hampered to go back into blood circulation by facilitating the enhanced permeability and retention (EPR) effect.[20] Therefore, T_1/T_2 switchable CAs have been assumed to be more beneficial for their effective tumor accumulation. In our previous work, two kinds of ESIONP-based T_1/T_2 switchable CAs were constructed and the aggregation strategy generated favorable MRI contrast effect at the tumor location owing to effective accumulation.[27-28] Additionally, the work that the ultrasmall iron oxide nanoparticles served as a T_2 contrast agent to specifically amplify the T_2 contrast signal originated from the aggregation in the tumor location has been reported.[29] Compared with this strategy, the T_1/T_2 switchable CAs that can specifically switch to a T_2 contrast agent may provide the totally different signal from initial contrast signal, resulting in great T_2 contrast enhancement and low background signal. Consequently, it would be more favorable to develop T_1/T_2 switchable CAs based on ESIONPs that are capable of switching from a T_1 contrast agent to a T_2 one for the precise tumor diagnosis.

Smart polymers that respond to the external stimuli such as pH, redox potential and enzyme have attracted intense interest in biological applications.[30-37] In particular, various pH-responsive polymers have been employed to construct stimulus-responsive nanoplatforms for tumor therapy and imaging.[38-40] Among them, polymer with sulfadimethoxine (SDM) groups show a very sharp transition range and remarkably pH-dependent solubility resulting from the ionization of the functional groups in the

acid tumor microenvironment (TME), providing a reasonable tactic to design stimulus-responsive CAs.[41-44] In addition, a special attention has been paid to the host-guest adamantane/β-CD (Ad/β-CD) complexation in the design of nanostructured materials, due to the strong association constant on account of the great fitness of Ad into β-CD cavity.[45-48] In the present work, we designed and prepared polysulfadimethoxine (PSDM)-modified ESIONPs based on the Ad/β-CD complexation as a pH-responsive T_1/T_2 switchable contrast agent to selectively activate T_2 MRI signal at the tumor region . Polyethylene glycol (PEG) terminally modified with adamantane (Ad-PEG-NH_2) was introduced on the surface of ESIONPs to obtain adamantane-modified ESIONPs (ESIONPs-PEG-Ad). Moreover, carboxylic acid-modified PSDM (PSDM-COOH), obtained by reversible addition-fragmentation chain transfer (RAFT) polymerization, was covalently bound to the amino functions present on β-CD molecule. The resulted macromolecule was conjugated with ESIONPs-PEG-Ad to form the pH-responsive T_1/T_2 switchable contrast agent ESIONPs-PEG-PSDM. Due to the hydrophilic property of PSDM at neutral pH, ESIONPs-PEG-PSDM is highly dispersed and affords T_1 contrast effect during blood circulation. After reaching the tumor acid environment, the PSDM on the surface of ESIONPs turn hydrophobic, leading to aggregation of the nanoparticles generating a negative T_2 signal. Therefore, with the accomplishment of aggregation, the T_1/T_2 switchable ESIONPs-PEG-PSDM will shift from a T_1 to a T_2 contrast agent, and T_2 contrast effect at tumor location will be selectively enhanced for the accurate diagnosis.

2. RESULTS AND DISCUSSION

Preparation and characterization of pH-induced aggregation of ESIONPs-PEG-PSDM. To construct pH-responsive ESIONPs-PEG-PSDM, the smart polymer PSDM-COOH was first synthesized by RAFT polymerization and then conjugated to amino β-CD molecule through the amidation reaction to obtain β-CD-PSDM.[41] In addition, adamantane group was introduced to the surface of ESIONPs through Ad-PEG-NH_2, performing the reaction between the amino group and the active pentafluorophenyl ester-modified ESIONPs (ESIONPs-PFP).[20] Fourier transform infrared (FTIR) spectroscopy was employed to confirm the structure of ESIONPs-PEG-Ad. The band around 1650 cm^{-1} is attributed to the amide bond derived from the amidation reaction between the PFP-activated COOH group on ESIONPs and the terminal amino group of PEG. Besides, the bands visible at 1108 cm^{-1} and 2894 cm^{-1} are ascribed to C-O-C and C-H from PEG chain, respectively (Figure S1). Then, ESIONPs-PEG-PSDM was obtained by the host-guest interaction using β-CD-PSDM and ESIONPs-PEG-Ad (Figure 1).

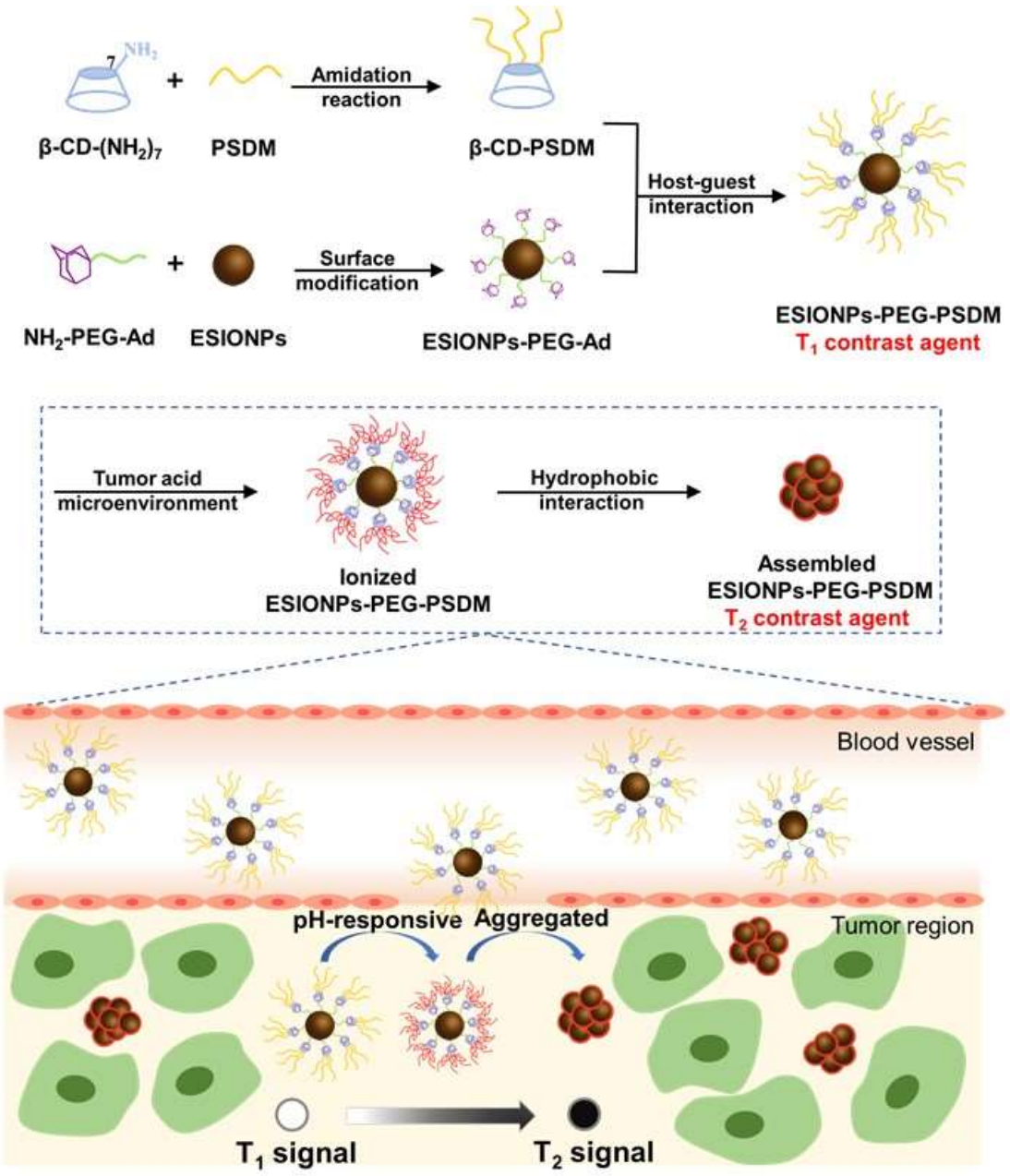

Figure 1. Schematic illustration for the preparation of ESIONPs-PEG-PSDM as a pH-responsive contrast agent and mechanism for switchable T_1/T_2 MRI in tumor acid microenvironment.

The structure of ESIONPs-PEG-PSDM was again verified through FTIR spectroscopy. As shown in Figure S2, the FTIR spectrum shows the characteristic peaks of amide bond (CO-NH) at 1592 cm^{-1}, and O=S=O bonds at 1360 cm^{-1}, 1140 cm^{-1} and

595 cm^{-1}, confirming the introduction of PSDM.[49] Following the preparation and characterization of the final complex, the pH-responsive aggregation properties of ESIONPs-PEG-PSDM were investigated by transmission electron microscope (TEM) and dynamic light scattering (DLS) in the neutral and weakly acid pH conditions. Before the investigation of pH-responsive aggregation, the stability of ESIONPs-PEG-PSDM in the aqueous solution was monitored. The hydrodynamic size remained constant in PBS (pH = 7.4) and cell culture medium (pH = 7.4), showing good stability of ESIONPs-PEG-PSDM (Figure S3). Following this evaluation, further investigations about pH-responsive aggregation were implemented. As shown in Figure 2a, the TEM image of ESIONPs-PEG-PSDM exhibits good dispersibility at pH = 7.4. When exposed to weakly acid environment (pH = 6.5), the obvious aggregation happens and the clusters of ESIONPs with big size can be clearly seen (Figure 2b). DLS characterization was further used to confirm the pH-dependent aggregation of ESIONPs-PEG-PSDM. The average hydrodynamic diameter of ESIONPs-PEG-PSDM is approximate 11 nm at pH = 7.4, while it reaches up to 190 nm at pH = 6.5, confirming the property of acid-responsive aggregation (Figure 2c). The aggregates are found to be relatively stable above certain concentration and less prone to disintegrate based on the hydrophobic interaction of surface PSDM(Figure S4 and S5). In addition, the zeta potential of ESIONPs-PEG-PSDM at pH = 7.4 and pH = 6.5 changed from -46.6 mV to -18.4 mV, indicating that the aggregation occurred along with the deionization of sulfonamide monomer units in the weakly acid condition (Figure S6). Moreover, as shown in the inserted image of Figure 2c, the pH-induced aggregation behavior can be observed

through the change of solution turbidity. The solution of ESIONPs-PEG-PSM is clear at pH = 7.4 and turns cloudy at pH = 6.5. Furthermore, the pH-induced aggregation profile was monitored at various pH values by DLS. As shown in Figure S7, the hydrodynamic size of ESIONPs-PEG-PSDM increases with the decrease of pH value, and the change of size exhibits a significant transition between pH = 6.6 and pH = 6.8 (Figure 2d). The transverse relaxation time (T_2) of ESIONPs-PEG-PSDM with an iron concentration of 0.15 mM in a range of pH values was also recorded using a 0.5 T NMR scanner at 35 ^{o}C, to investigate the transition point. The T_2 value has a value around 320 ms at the pH range of 6.6-7.4 and then sharply drops to 145.8 ms at pH = 6.6, and 87 ms at pH 6.4. It is obvious that ESIONPs-PEG-PSDM shows a sharp conversion from dispersed to aggregated situation based on the pH-responsive hydrophilic to hydrophobic transition with the transition point occurring around pH = 6.7, as previously reported.[50] Besides, the T_2 value remained stable during 12 h at pH = 6.5, implying that there is no cluster disassembly (Figure S8). Overall, the pH-responsive morphological and hydrodynamic size changes, as well as the variation of T_2 value prove the conversion from dispersed ESIONPs to clustered particles under the weakly acid condition.

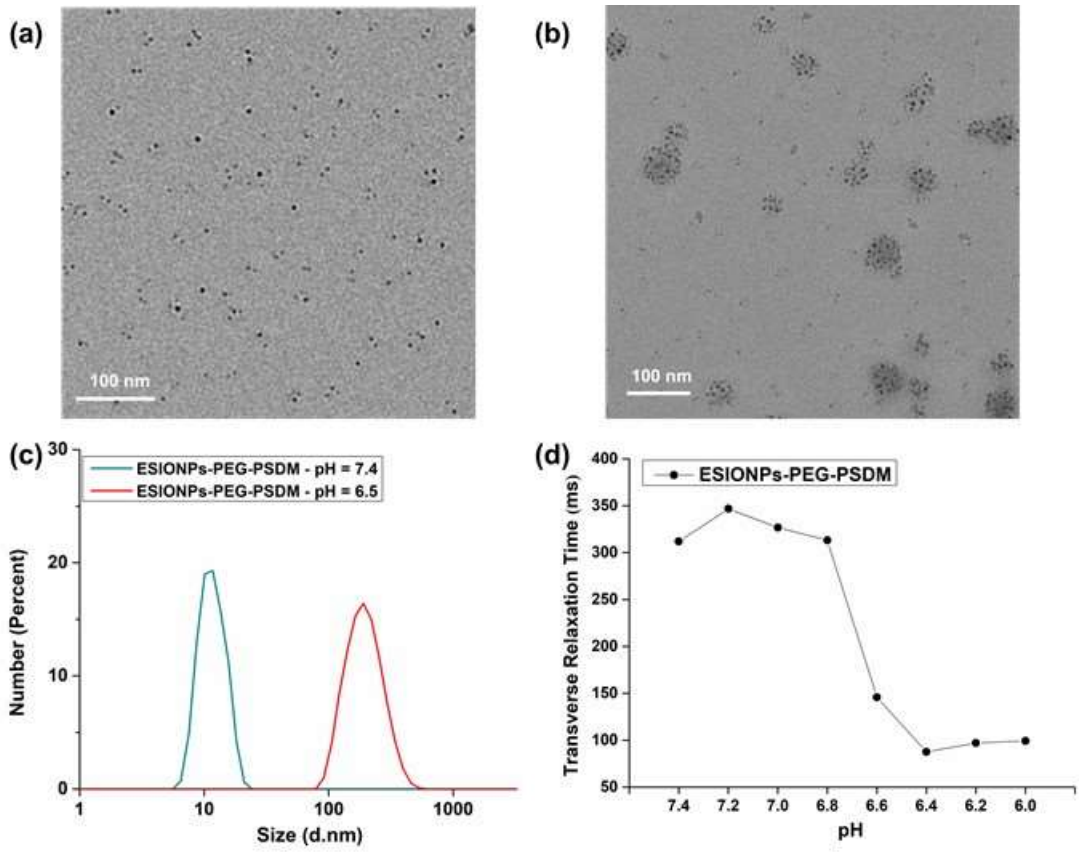

Figure 2. TEM images of ESIONPs-PEG-PSDM (a) at pH = 7.4 and (b) at pH = 6.5. (c) Hydrodynamic diameter distribution of ESIONPs-PEG-PSDM at pH = 7.4 and pH = 6.5. (d) T_2 variation for ESIONPs-PEG-PSDM with an iron concentration of 0.15 mM at the pH range of 7.4-6.0.

Investigation on pH-responsive relaxation property of ESIONPs-PEG-PSDM. To estimate the MRI signal switching performance, ESIONPs-PEG-PSDM was diluted into a series of iron concentrations at pH = 7.4 and pH = 6.5 followed with the measurement of relaxation time at 35 ^{o}C on a 0.5 T NMR scanner. The longitudinal and transversal relaxivity (r_1 and r_2) values under different pH conditions were calculated by the slope plots. As shown in Figure 3a and 3b, the r_1 and r_2 values at pH = 7.4 correspond to 3.37 $mM^{-1}s^{-1}$ and 8.72 $mM^{-1}s^{-1}$, respectively. Decreasing the pH to 6.5,

the r_1 value of ESIONPs-EPG-PSDM slightly decreases to 1.25 $mM^{-1}s^{-1}$, while r_2 value shows a remarkable increase to 33.4 $mM^{-1}s^{-1}$. It is clear that ESIONPs-PEG-PSDM reaches the high r_2/r_1 ratio of 26.7 at pH = 6.5 compared with that of 2.58 at pH = 7.4, indicating a clear conversion from a T_1 to T_2 contrast agent. Moreover, the relaxation times were also measured at 35 ºC on a 1.5 T NMR scanner. The r_2/r_1 ratio converts from 7.24 to 22.42 when pH value is adjusted from 7.4 to 6.5, which also confirms the switch from a T_1 to T_2 contrast agent (Figure S9).[51,52] Additionally, the T_1 and T_2-weighted magnetic resonance phantom images at different pH conditions (pH = 7.4 and pH = 6.5) were collected on a 0.5 T NMR scanner to verify the switch of contrast agent type (Figure 3c and 3d). For T_1-weighted imaging, the lightness of phantom image improves with the increase of iron concentration at pH = 7.4. This typical concentration dependent T_1 effect indicates that ESIONPs-PEG-PSDM is a T_1 contrast agent around neutral pH conditions.[19] At the same time, the lightness of T_2-weighted images shows negligible change with the increase of iron concentration. Moreover, T_2-weighted image at pH = 6.5 becomes darker with raising the iron concentration, demonstrating that T_2 contrast effect has been activated based on the pH-responsiveness. Therefore, ESIONPs-PEG-PSDM with improved T_2 contrast enhancement in a concentration-dependent manner can be considered a typical T_2 contrast agent at pH = 6.5.[53] Simultaneously, the lightness variation of T_1-weighted images with the increase of iron concentration can be ignored at pH = 6.5. The variation of the relaxivities and the presentation of T_1 and T_2-weighted images at different pH confirm that ESIONPs-PEG-PSDM can response to weakly acid environment changes and switch from a T_1 contrast

agent to a T_2 one.

The mechanisms behind the T_1/T_2 switch for ESIONPs-PEG-PSDM can be explained as follows. On the basis of Solomon-Bloembergen-Morgan (SBM) theory and Freed theory, r_1 is related to the contribution of water molecule in the inner sphere and outer sphere.[54] The influence of inner sphere on r_1 mainly arise from the number of water molecules q and their residence time τ_M in the first coordination sphere, while the important fact of outer sphere affecting r_1 is the diffusion correlation time of water molecules τ_D (detailed theoretical equations are provided in Supporting Information). ESIONPs-PEG-PSDM is well dispersed with hydrophilic PEG and PSDM polymer coated on the surface at pH 7.4, while it tends to aggregate at the weakly acid condition following the decrease of r_1.[41-43] For the contribution from inner sphere, the change of r_1 is derived from the lower surface/volume ratio of nanoparticles after aggregation leading to the decrease of hydration number of surface Fe^{3+} ions on ESIONPs. In the case of the influence from outer sphere, with the lower water permeability of polymer shell after aggregation, the approach of water molecules to iron oxide surface is impeded, resulting in higher τ_D in outer sphere, which also decreases r_1. On the other hand, the main determining parameters for r_2 are saturation magnetization M_s and impermeable layer around superparamagnetic core L (detailed theoretical equations are provided in SI).[55] Both M_s and L will increase with the aggregation of ESIONPs after exposure to the weakly acid environment, which leads to the enhancement of r_2. In summary, the decrease of r_1 and the increase of r_2 after the pH-responsive aggregation contribute to the conversion from T_1 to T_2 contrast effect.

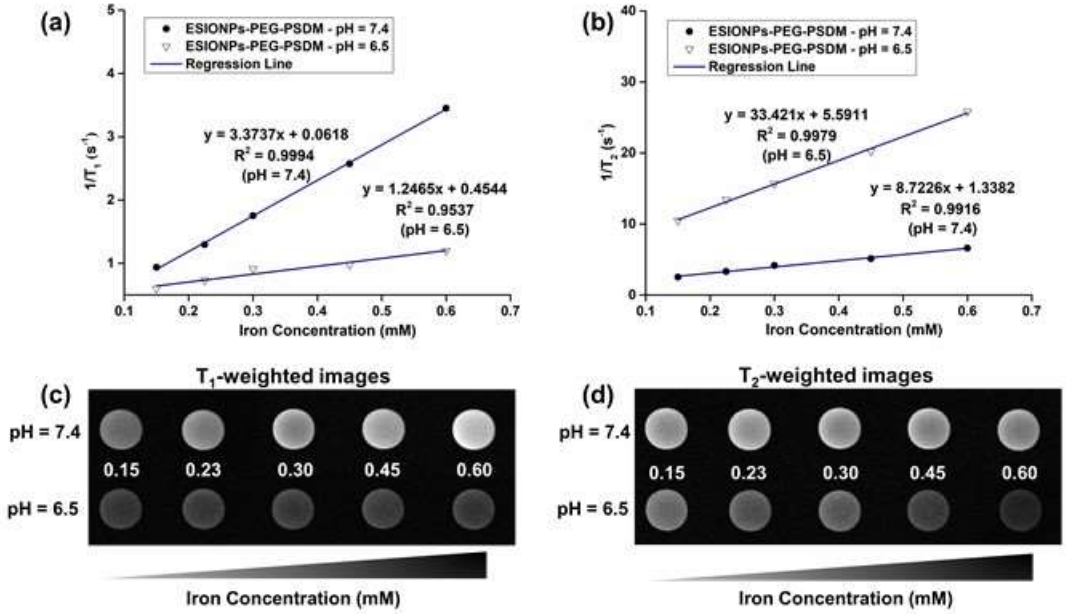

Figure 3. Plots of (a) inverse longitudinal relaxation time ($1/T_1$) and (b) inverse transverse relaxation time ($1/T_2$) as a function of iron concentration for ESIONPs-PEG-PSDM at pH = 7.4 and pH = 6.5. (c) T_1-weighted and (d) T_2-weighted phantom images of ESIONPs-PEG-PSDM at various iron concentrations, at pH = 7.4 and pH = 6.5.

Confirmation of T_1/T_2 switchable MRI contrast on tumor-bearing mice. To investigate the tunable MRI contrast effect, a tumor-bearing mice model was established and ESIONPs-PEG-PSDM with an iron dose of 0.1 mmol/kg was intravenously injected. The T_1-weighted and T_2-weighted MR images were recorded on a 1.5 T scanner at various time points. As shown in the Figure 4a, the lightness of T_1-weighted MR images located at the tumor region improves slightly at the time points of 2 h and 4 h, and there is a clear decrease of brightness at 6 h, which may be ascribed to the reduced T_1 contrast effect after the gradual aggregation of ESIONPs. For T_2-weighted MR images of ESIONPs-PEG-PSDM, the lightness at tumor location becomes darker with the increase of time, meaning that the T_2 MRI contrast has been

activated. At the time point of 6 h, the T_2 signal intensity is visibly enhanced with the low background signal, revealing the T_1/T_2 switch of ESIONPs-PEG-PSDM is beneficial for the accurate tumor diagnosis. Besides, the aggregated clusters can be clearly seen from the TEM images of tumor tissues after the intravenous injection of ESIONPs-PEG-PSDM, implying the formation of clustered ESIONPs and the activation of T_2 MRI signal (Figure 5). To quantitatively evaluate the contrast enhancement, the signal intensity ratio of the tumor site was analyzed by ImageJ software. For the signal intensity ratio of T_1-weighted MR images, the ratio value is 113.6 ± 1.2% at 6 h and the T_1 contrast signal is barely enhanced, regardless of the slightly increase to around 126% at 2 h which may be ascribed to the gradual T_1/T_2 switch (Figure 4b). Furthermore, as shown in Figure 4c, the T_2 contrast signal is obviously improved at 6 h according to the large decrease of signal intensity ratio (56.4 ± 2.7%), which further confirms that ESIONPs-PEG-PSDM with pH-responsiveness can aggregate at the tumor location and convert to a T_2 contrast agent. Moreover, to better understand the quantitative distribution of the nanoparticles during imaging, the accumulated amount in main organs and tumors at 6 h after intravenous injection were investigated based on the inductively coupled plasma atomic emission spectrometer (ICP-OES) measurements. As shown in Figure S10, the accumulated content in the tumor tissue is about 29.4 ± 9.7 %ID/g. At the same time, the accumulated amounts in reticuloendothelial system organs, including liver and spleen, are comparable to those in tumor tissue, similarly to the results in the published literatures.[56] Additionally, ESIONPs-PEG-PSDM was directly injected into the tumor and into a muscle tissue to

further investigate the signal switch based on the pH-responsiveness (Figure S11). After intra-tumor injection, the T_2-weighted image exhibits a significant darkened signal at the tumor region, while that of muscle-injected group presents oppositely a brightened signal at the tissue location. The different phenomenon is contributed to the pH-induced T_1/T_2 switch of ESIONPs-PEG-PSDM.[57] After 24 h injection, the T_1 contrast enhancement is negligible, while T_2 signal is slightly enhanced as the lightness at tumor site is decreased (Figure S12). Overall, pH-responsive ESIONPs-PEG-PSDM are able switch from a T_1 to T_2 contrast and to enhance the T_2 contrast effect at the tumor acid environment.

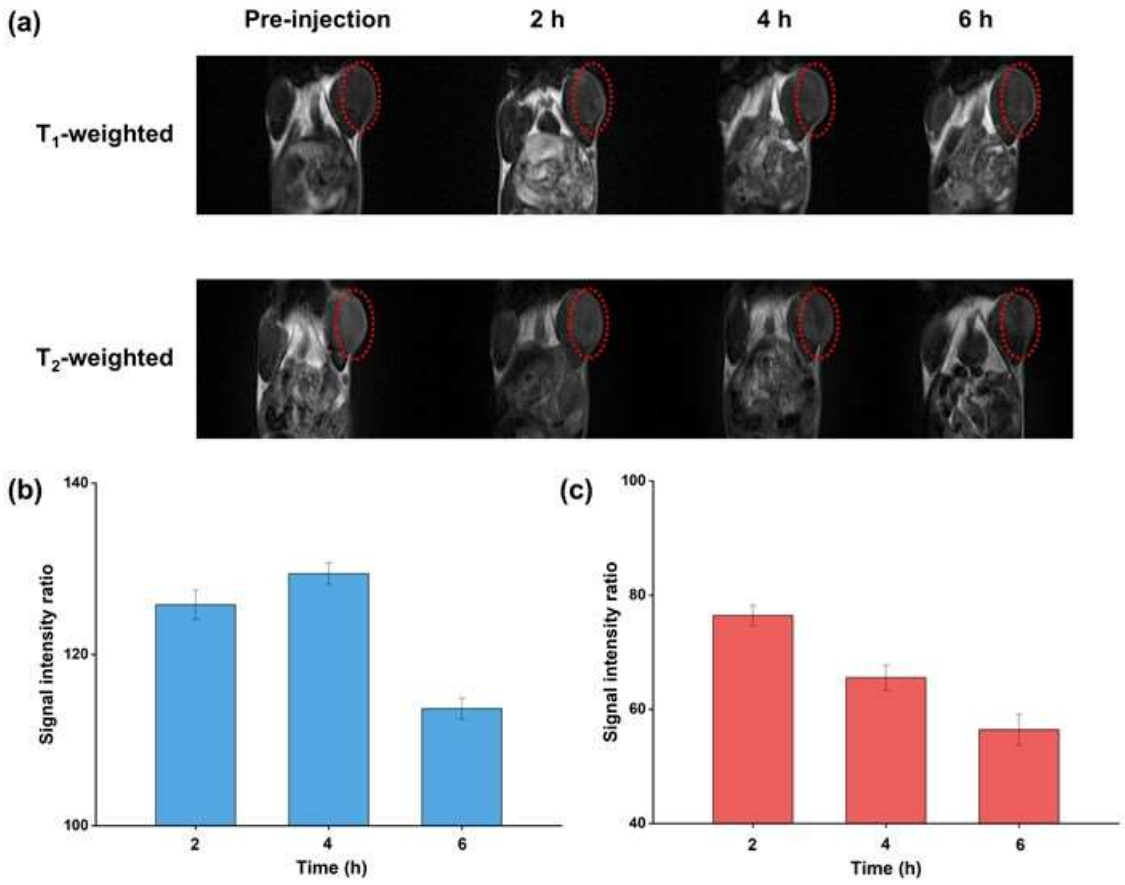

Figure 4. (a) T_1-weighted and T_2-weighted MR images of tumor-bearing mice before and after intravenously injection with ESIONPs-PEG-PSDM at an iron dose of 0.1

mmol/kg. The red dashed circles indicate the tumor region. Quantitative analysis of signal intensity ratio of (b) T_1-weighted and (c) T_2-weighted MR images at various time points. The signal intensity ratio was calculated based on the scale of the gray values obtained using Image J. The signal intensity (SI) ratio of the tumor region was calculated by SI post-injection/SI pre-injection.

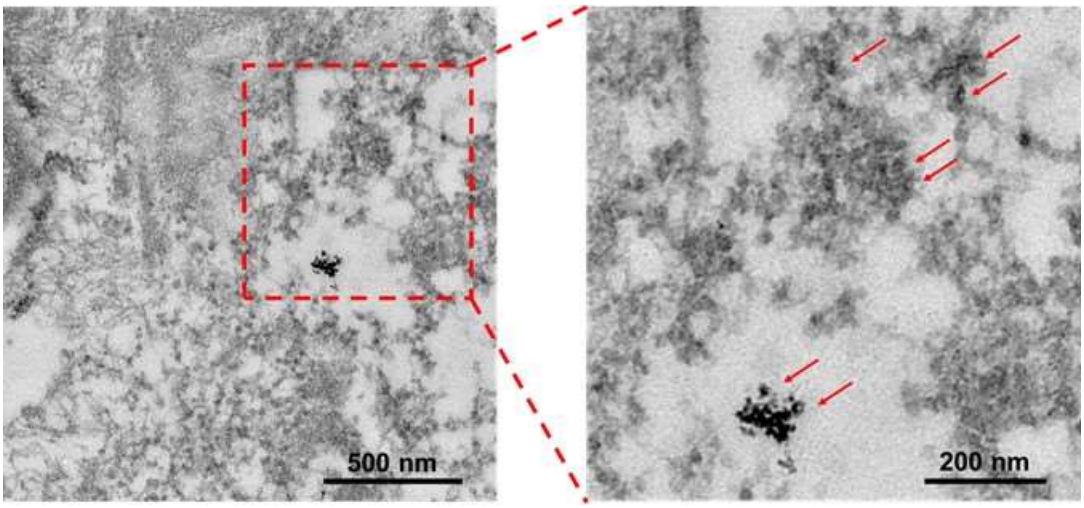

Figure 5. TEM images of tumor tissues obtained from mice injected with ESIONPs-PEG-PSDM. ESIONPs-PEG-PSDM was intravenously into mice at an iron dose of 0.1 mmol/kg and sacrificed at 6 h. Red arrows indicate the aggregation of ESIONPs.

Biosafety and biodistribution of ESIONPs-PEG-PSDM. The biocompatibility is of great importance for the construction of potential CAs for clinical application. To evaluate the biosafety and biocompatibility, cytotoxicity and tissue toxicity assays were performed. ESIONPs-PEG-PSDM sample with a series of iron concentration were incubated with human umbilical vein endothelial cells (HUVEC) and 4T1 mouse breast cancer cells for 24 h, respectively, and then cell viability of each group was obtained by WST test. As shown in Figure 6, the viability values of HUVEC cells are all higher

than 90%. Even when the iron concentration is as high as 2 mM, the proportion of viable cell is 97.5 ± 4.6 %. Similarly, the cell viability values of 4T1 cells after incubation for 24 h are all above 90%, and the value is 94.8 ± 2.3 % at an iron concentration of 2 mM, showing the negligible cytotoxicity of ESIONPs-PEG-PSDM.

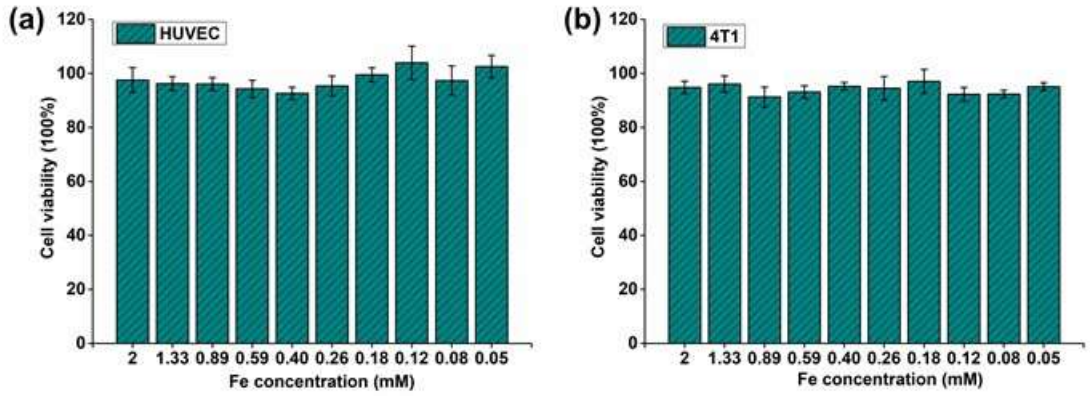

Figure 6. Cell viability of (a) HUVEC and (b) 4T1 cells after incubated with ESIONPs-PEG-PSDM at various iron concentrations for 24 h.

Moreover, after the intravenous injection of ESIONPs-PEG-PSDM at an iron dose of 0.1 mmol/kg, mice were sacrificed and the main organs (heart, liver, spleen, lung, kidney and tumor) were collected for histological assessment (Figure 7). Compared with blank group that underwent an intravenous injection of physiological saline, there are no necrosis, inflammation or any other adverse influence of the nanoparticles in the hematoxylin-eosin (H&E) staining images of ESIONPs-PEG-PSDM treated group. Overall, the results of cytotoxicity and tissue toxicity tests indicate that ESIONPs-PEG-PSDM is endowed of a favorable biocompatibility and has great potential for the biomedical application.

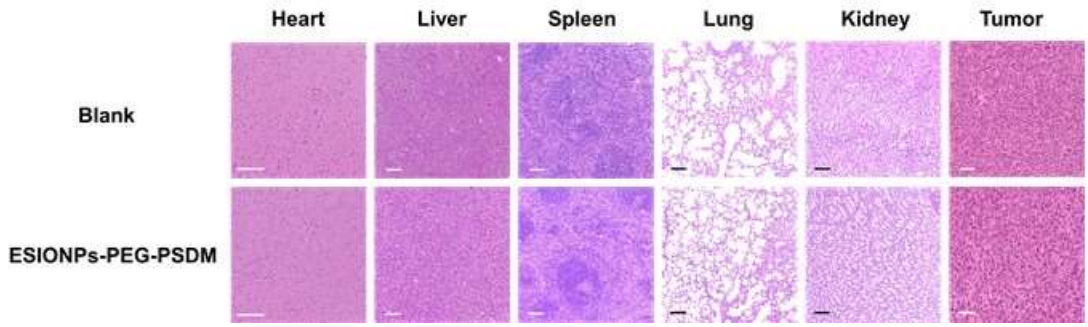

Figure 7. H&E staining images of heart, liver, spleen, lung, kidney and tumor. The mice were intravenously injected with ESIONPs-PEG-PSDM at an iron dose of 0.1 mmol/kg and sacrificed at 72 h. The mice intravenously injected with physiological saline served as blank group. The scale bar is 100 μm.

In addition, mice were sacrificed after 7 days and 14 days after intravenous injection of ESIONPs-PEG-PSDM at an iron dose of 0.1 mmol/kg and the main organ tissues were collected to analyze the biodistribution of the material. Figure 8 shows that the majority of the iron ion are accumulated into spleen, with an iron content of 13.2 ± 6.1 %ID/g at the time point of 7 days. A few other iron ions are concentrated in the heart, liver and kidney tissues. After injection for 14 days, the content of iron ion into spleen decreases to 1.4 ± 1.1 %ID/g, implying that the iron ions in the main organs are eventually cleared out of the organ. In a whole, the biosafety and biodistribution characterization demonstrate ESIONPs-PEG-PSDM is a potential contrast agent with favorable biological security.

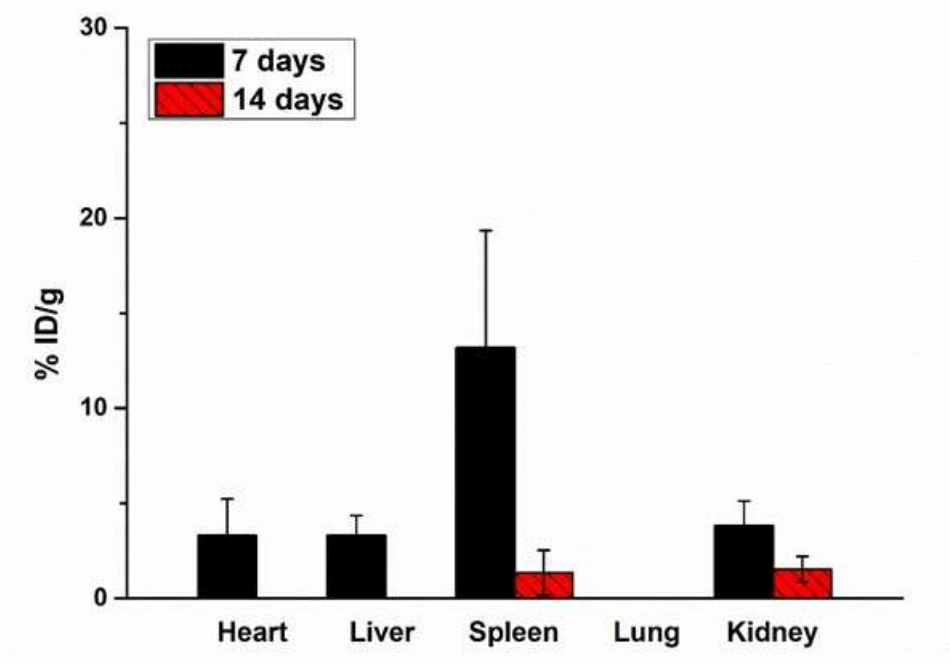

Figure 8. Biodistribution of ESIONPs-PEG-PSDM at the time point of 7 days and 14 days after intravenously injected with ESIONPs-PEG-PSDM at an iron dose of 0.1 mmol/kg.

3. CONCLUSION

In summary, we designed and constructed a pH-responsive contrast agent ESIONPs-PEG-PSDM that can respond to tumor acid environment, tuning the T_1 and T_2 relaxation properties based on conjugating pH-sensitive PSDM polymer onto the surface of ESIONPs via host-guest interaction. The dispersed ESIONPs-PEG-PSDM with extremely small size acts as T_1 contrast agent in the neutral environment. While in response to the acid environment, the surface PSDM polymer transforms from hydrophilic to hydrophobic and the ESIONPs aggregate to clusters, resulting in the switch to a T_2 contrast agent. Moreover, the T_1/T_2 signal switchable property was also verified in the tumor region. Finally, ESIONPs-PEG-PSDM, equipped with favorable biocompatibility and sensitive responsiveness, can selectively activate T_2 MRI contrast

effect at the tumor site and may provide a promising platform for an accurate diagnosis of tumors.

4. EXPERIMENTAL SECTION

Materials and Characterizations. Dichloromethane (DCM, Sinopharm) was dried overnight with CaH_2 and distilled before use. Pentafluorophenol, trifluoroacetic acid (TFA), methacryloyl chloride, succinic anhydride and 1-amantadine were purchased form Adamas-beta. N,N-Diisopropylethylamine (DIPEA), sulfadimethoxine and 2,2′-azobis(isobutyronitrile) (AIBN) were supplied by TCI. N,N'-dicyclohexylcarbodiimide (DCC) was obtained from J&K Chemical Reagent Company. 4-Cyano-4-(thiobenzoylthio) pentanoic acid (CTP) was purchased from Energy Chmeical. All-amino β-CD was supplied by Shandong Binzhou Zhiyuan Bio-Technology Co., Ltd. NH_2-PEG-Boc (average Mn = 2000) was purchased from Ponsure Biotechnology. Other reagents were obtained from Sinopharm. 4-((adamantan-1-yl)amino)-4-oxobutanoic acid (Ad-COOH) was synthesized by the method previously reported in the literature and the chemical structure was confirmed by the ^{1}H NMR spectrum (Figure S13).[58] ESIONPs-PFP was prepared according to our previous publication.[20]

All ^{1}H nuclear magnetic resonance (NMR) spectra data were obtained from a 400 MHz NMR spectrometer (Varian). Fourier transform infrared (FTIR) spectra were recorded on an FTIR spectrometer (Thermo Fisher). The weight-average molecular weight (M_w) and number-average molecular weight (M_n) of polymer were obtained from the gel permeation chromatography (GPC) system with dimethyl sulfoxide

(DMSO) as the eluent. Iron concentrations were determined by an inductively coupled plasma atomic emission spectrometer (ICP-OES, Thermo Fisher). Dynamic light scattering (DLS, Malvern Instruments) were used to provide the hydrodynamic size. Transmission electron microscope (TEM) images were collected by a TEM equipment (120 kV, Hitachi-HT7700). The relaxation times were monitored on a 0.5 T NMR scanner (Shanghai Huantong Science and Education Equipment Co., Ltd, GY-PNMR-10). In vivo MRI was acquired on a 1.5 T scanner (Shanghai Huantong Science and Education Equipment Co., Ltd, HT-MRSI60-35A). WST assay was employed to detect the cytotoxicity of cells (Biotek citation 3).

Synthesis of the pH-responsive polymer PSDM-COOH. The methacryloyl sulfadimethoxine was synthesized according to a published protocol.[50] Briefly, sulfadimethoxine (15 g, 48.4 mmol) was dissolved in 100 mL mixture of 0.25 M NaOH and acetone (1:1), followed by addition dropwise of methacryloyl chloride (4.84 mL, 50.3 mmol) in an ice bath. The reaction mixture was stirred for 2 h and the precipitation was collected by filtration. After washing with deionized water, the purified solid was recrystallized in methanol. The white product methacryloyl sulfadimethoxine was dried under vacuum oven overnight and the chemical structure was confirmed by the ^{1}H NMR spectrum (Figure S14). ^{1}H-NMR (DMSO-d6): 11.5 (1H, -SO_2-N***H***-), 10.2 (1H, -CO-N***H***-), 7.9 (4H, aromatic group), 6.0-5.8 (2H, -CH_3-C(C***H***$_2$)-), 5.6 (1H, 2-pyrimidine), 3.8-3.7 (6H, C***H***$_3$-O-), 1.96 (3H, C***H***$_3$-C(CH_2)-).

PSDM-COOH was synthesized through RAFT polymerization.[41] The methacryloyl sulfadimethoxine (4.42 g, 1.89 mmol), CTP (21.78 mg, 0.078 mmol) and AIBN (4.4

mg, 0.027 mmol) were dissolved in 10 mL DMSO in a Schlenk flask. After degassing with three freeze-pump-thaw cycles, the reaction temperature was raised to 70 ℃ and stirred under argon atmosphere for 24 h. After this step, the solution was poured into cold diethyl ether and the precipitation was wash with diethyl ether for three times. The ^{1}H NMR spectrum of COOH-PSDM was shown in the Figure S15. ^{1}H-NMR (DMSO-d6): 11.5 (1H, -SO_2-N***H***-), 9.5 (1H, -Ph-N***H***-), 8.0-7.5 (4H, aromatic group), 5.9 (1H, 2-pyrimidine), 4.0-3.5 (6H, C***H***$_3$-O-).

Synthesis of polysulfadimethoxine-modified β-CD (β-CD-PSDM). The β-CD-PSDM was synthesized through an amidation reaction. PSDM-COOH (400 mg, 0.17 mmol), amino β-CD (10.14 mg, 0.10 mmol), 1-hydroxybenzotriazole (9.35 mg, 0.07 mmol) and DCC (14.26 mg, 0.07 mmol) were dissolved in 20 mL DMF and reacted at room temperature for 24 h. The residue was removed by filtration and the solution was dropped into diethyl ether to obtain white solid. The precipitation was dissolved in a NaOH aqueous solution (pH = 8.0) and dialyzed (MWCO: 7000 Da) against water (adjusted to pH = 8.0 with 1 M NaOH) for 3 days. Finally, the product was achieved by lyophilization and the successful conjugation of PSDM-COOH to amino β-CD was confirmed by GPC (Figure S16).

Synthesis of pentafluorophenyl 4-((adamantan-1-yl)amino)-4-oxobutanonate (Ad-PFP). Ad-COOH (2.0 g, 7.96 mmol) and pentafluorophenol (1.47 g, 9.54 mmol) were dissolved in 50 mL 1,4-dioxane. Then, DCC (2.0 g, 9.70 mmol) in 10 mL 1,4-dioxane was dropped into the Ad-COOH solution and stirred under argon atmosphere at room temperature overnight. The reaction mixture was filtered and the solution was

removed by a rotary evaporator. The final product was obtained through column chromatography using a silica column with DCM as eluant. The chemical structure of Ad-PFP was confirmed by the ^{1}H NMR spectrum (Figure S17). ^{1}H-NMR ($CDCl_3$): 5.3 (1H, Ad-N***H***-), 3.0 (2H, -NHCO-CH_2-C***H***$_2$-), 2.6 (2H, -NHCO-C***H***$_2$- CH_2-), 2.2-1.9 (9H, adamantane), 1.4 (6H, 1-cyclohecane).

Synthesis of Ad-PEG-NH_2. NH_2-PEG-Boc (500 mg, 0.25 mmol) and Ad-PFP (200 mg, 0.46 mmol) were dissolved in 15 mL DCM, followed by addition of DIPEA (436 μL, 2.5 mmol). The reaction mixture was stirred at room temperature under nitrogen atmosphere for 24 h and precipitated in diethyl ether. The white product was dried under vacuum oven. Afterwards, Ad-PEG-Boc (450 mg, 0.22 mmol) and TFA (5 ml, 65.30 mmol) were stirred in 10 mL DCM in an ice bath for 2 h. The solution was dropped into diethyl ether to obtain precipitation. The final product was dried under vauum oven and the ^{1}H NMR spectra of Ad-PEG-Boc and Ad-PEG-NH_2 were shown in the Figure S18 and S19. ^{1}H-NMR ($CDCl_3$): 3.8-3.5 (-(C***H***$_2$C***H***$_2$O)-), 2.2-2.0 (9H, adamantane), 1.7 (6H, 1-cyclohecane), 1.5 (9H, -C(C***H***$_3$)$_3$).

Preparation of ESIONPs-PEG-Ad. Ad-PEG-NH_2 (200 mg, 0.10 mmol) and 30 mg ESIONPs-PFP were dissolved in 30 mL DCM.[19] Then, DIPEA (436 μL, 2.5 mmol) was added into the reaction mixture and stirred at room temperature for 24 h. After reaction, the solution was poured into pure diethyl ether, the ESIONPs-PEG-Ad was collected by centrifugation and dissolved in deionized water for later use.

Host-Guest Assembly of ESIONPs-PEG-PSDM. The ESIONPs-PEG-PSDM was

prepared through host-guest interaction. One hundred mg PSDM-COOH and 20 mg ESIONPs-PEG-Ad were dissolved in NaOH aqueous solution (pH = 8.0) and stirred at room temperature overnight. The reaction mixture was dialyzed (MWCO: 35000 Da) against water (adjusted to pH = 8.0 with 1 M NaOH) for 3 days. The final product was achieved by lyophilization.

Characterization of pH-induced aggregation property. The pH-dependent responsiveness of ESIONPs-PEG-PSDM was investigated by TEM and DLS. ESIONPs-PEG-PSDM was dispersed in 0.1 M PBS (phosphate-buffered saline) at pH = 7.4 and pH = 6.5 with an iron concentration of 1 mM. The morphologies of the assembled and disassembled nanoparticles were observed by TEM. In parallel, ESIONPs-PEG-PSDM was dispersed in 0.1 M PBS at pH = 7.4 and pH = 6.5 with an iron concentration of 0.5 mM and the size distribution of each sample was obtained by DLS instrument. In addition, ESIONPs-PEG-PSDM was diluted in PBS at various pH values (6;0-7.4), then the hydrodynamic size and T_2 value were acquired on a DLS instrument and a 0.5 T NMR scanner, respectively. For the measurements of T_2 relaxation time, Carr Purcell Meiboom Gill (CPMG) method (non-gated sequence, number of echoes TE = 334 ms, TR = 2000 ms and NS = 1) were employed.

Measurement of T_1 and T_2 relaxation time. The T_1 and T_2 relaxation time of ESIONPs-PEG-PSDM in PBS at pH = 7.4 and pH = 6.5 with various iron concentrations were recorded on a 0.5 T and 1.5 T NMR scanner maintaining the temperature at 35 ^{o}C. For the measurements of T_1 and T_2 relaxation time, inversion recovery and Carr Purcell Meiboom Gill (CPMG) method were respectively employed.

The r_1 and r_2 were calculated from the plots of curve-fitting results of the inverse relaxation time and iron concentration. Moreover, the T_1-weighted and T_2-weighted MRI phantom images of ESIONPs-PEG-PSDM in PBS at pH = 7.4 and pH = 6.5 with various iron concentrations were observed on a 0.5 T NMR scanner. The parameters of T_1-weighted MRI were set as follows: echo time (TE) = 134 ms, repetition time (TR) = 500 ms, number of scans (NS) = 1. The parameters of T_2-weighted MRI were set as follows: TE = 334 ms, TR = 2000 ms and NS = 1.

In vivo MRI study of T_1/T_2 switchable ESIONPs-PEG-PSDM. Tumor-bearing mice were observed before injection to obtain pre-injection T_1-weighted and T_2-weighted MR images. After that, ESIONPs-PEG-PSDM was intravenously injected into tumor-bearing mice at an iron dose of 0.1 mmol/kg. The T_1-weighted and T_2-weighted MR images were monitored at the time points of 2 h, 4 h and 6 h. The detailed procedures are shown in the Supporting Information.

Biocompatibility assay. WST assay was employed to evaluate the cytotoxicity of ESIONPs-PEG-PSDM. Briefly, ESIONPs-PEG-PSDM at various iron concentrations was incubated with 4T1 cells and human umbilical vein endothelial cells (HUVEC) for 24 h. The cell viability was calculated based on the WST assay. The details are shown in the Supporting Information. Besides, ESIONPs-PEG-PSDM was intravenously injected into mice at an iron dose of 0.1 mmol/kg. The mice were sacrificed after injected for 72 h and the main organ tissues were achieved for hematoxylin-eosin (H&E) staining images. Moreover, mice were injected with ESIONPs-PEG-PSDM and sacrificed after 7 days and 14 days to analyzed the biodistribution in vivo. The details

are shown in the Supporting Information.

ASSOCIATED CONTENT

Supporting Information

The Supporting Information is available free of charge on the ACS Publications website at DOI: pubs.acs.org.

Detailed information of the procedures for cell viability and animal experiments, *in vivo* MRI study; FTIR spectra of ESIONPs-PEG-Ad, β-CD-PSDM and ESIONPs-PEG-PSDM; hydrodynamic size of ESIONPs-PEG-PSDM at pH between 6.0 and 7.4; comparison of T_2-weighted MR images of ESIONPs-PEG-PSDM after its local injection in muscle and tumor; ^{1}H NMR spectra of Ad-COOH, methacryloyl SDM, PSDM, Ad-PFP, Ad-PEG-NH_2-Boc, Ad-PEG-NH_2; GPC analysis of PSDM and β-CD-PSDM.

ACKNOWLEDGMENTS

This work was financially supported by National Natural Science Foundation of China (22177129, 31900999, 32071392), Natural Science Foundation of Jiangxi Province (20192ACBL21055), the Science and Technology Project of Suzhou (SZS201904), and China Postdoctoral Science Foundation (2021M702405). Y. H. is grateful to Chinese Scholarship Council (CSC) for supporting her PhD at the University of Strasbourg. We also gratefully acknowledge the Centre National de la Recherche Scientifique (CNRS).

REFERENCES

(1) Garcia-Hevia, L.; Banobre-Lopez, M.; Gallo, J. Recent Progress on Manganese-Based Nanostructures as Responsive MRI Contrast Agents. *Chem.-Eur. J.* **2019**, 25 (2), 431-441.

(2) Zou, Y. B.; Jin, H. L.; Sun, F.; Dai, X. M.; Xu, Z. S.; Yang, S. L.; Liao, G. F. Design and Synthesis of a Lead Sulfide Based Nanotheranostic Agent for Computer Tomography/Magnetic Resonance Dual-Mode-Bioimaging-Guided Photothermal Therapy. *ACS Appl. Nano Mater.* **2018**, 1 (5), 2294–2305.

(3) Mo, Z. M.; Qiu, M. J.; Zhao, K. Z.; Hu, H.; Xu, Q.; Cao, J. G.; Luo, Y. X.; Liu, L. P.; Xu, Z. S.; Yi, C. F.; Xiong, Z. F.; Liao, G. F.; Yang, S. L. Multifunctional Phototheranostic Nanoplatform based on Polydopamine-Manganese Dioxide-IR780 Iodide for Effective Magnetic Resonance Imaging-Guided Synergistic Photodynamic/Photothermal Therapy. *J. Colloid Interface Sci.* 2022, 611, 193–204.

(4) Sun, W.; Thies, S.; Zhang, J.; Peng, C.; Tang, G.; Shen, M.; Pich, A.; Shi, X. Gadolinium-Loaded Poly(N-vinylcaprolactam) Nanogels: Synthesis, Characterization, and Application for Enhanced Tumor MR Imaging. *ACS Appl. Mater. Interfaces* **2017**, 9 (4), 3411-3418.

(5) Cai, W.; Zhang, Y.; Wang, J.; Wang, Z.; Tian, Y.; Liu, H.; Pan, H.; Fu, L.; Chen, W.; Wu, C.; Wang, X.; Liu, G. Engineering the Surface of Gd_2O_3 Nanoplates for Improved T_1-Weighted Magnetic Resonance Imaging. *Chem. Eng. J.* **2020**, 380, 122473.

(6) Davies, G. L.; Kramberger, I.; Davis, J. J. Environmentally Responsive MRI Contrast Agents. *Chem. Commun.* **2013**, 49 (84), 9704-9721.

(7) Fu, S. X.; Cai, Z. Y.; Ai, H. Stimulus-Responsive Nanoparticle Magnetic Resonance Imaging Contrast Agents: Design Considerations and Applications. *Adv. Healthcare Mater.* **2021**, 10 (5), 2001091.

(8) Ma, T.; Zhang, P.; Hou, Y.; Ning, H.; Wang, Z.; Huang, J.; Gao, M. "Smart" Nanoprobes for Visualization of Tumor Microenvironments. *Adv. Healthcare Mater.* **2018**, 7 (20), e1800391.

(9) Yoo, B.; Pagel, M. D. An Overview of Responsive MRI Contrast Agents for Molecular Imaging. *Front. Biosci.* **2008**, 13, 1733-1752.

(10) Hsieh, V.; Okada, S.; Wei, H.; Garcia-Alvarez, I.; Barandov, A.; Alvarado, S. R.; Ohlendorf, R.; Fan, J. X.; Ortega, A.; Jasanoff, A. Neurotransmitter-Responsive Nanosensors for T_2-Weighted Magnetic Resonance Imaging. *J. Am. Chem. Soc.* **2019**, 141 (40), 15751-15754.

(11) Gao, Z.; Hou, Y.; Zeng, J.; Chen, L.; Liu, C.; Yang, W.; Gao, M. Tumor Microenvironment-Triggered Aggregation of Antiphagocytosis (99m) Tc-Labeled Fe_3O_4 Nanoprobes for Enhanced Tumor Imaging In Vivo. *Adv. Mater.* **2017**, 29 (24), 1701095.

(12) Anju, S.; Ashtami, J.; Mohanan, P. V. Black phosphorus, A Prospective Graphene Substitute for Biomedical Applications. *Mater. Sci. Eng., C* **2019**, 97, 978-993.

(13) Yuan, Y.; Ding, Z.; Qian, J.; Zhang, J.; Xu, J.; Dong, X.; Han, T.; Ge, S.; Luo, Y.; Wang, Y.; Zhong, K.; Liang, G. Casp3/7-Instructed Intracellular Aggregation of Fe_3O_4 Nanoparticles Enhances T_2 MR Imaging of Tumor Apoptosis. *Nano. Lett.* **2016**,

16 (4), 2686-2691.

(14) Huang, Z. X.; Wang, Y. J.; Wu, M.; Li, W. T.; Zuo, H.; Xiao, B.; Zhang, X. Q.; Wu, J.; He, H. W.; Xia, Q. Y. Sericin-Based Gadolinium Nanoparticles as Synergistically Enhancing Contrast Agents for pH-Responsive and Tumor Targeting Magnetic Resonance Imaging. *Mater. Des.* **2021**, 203, 109600.

(15) Li, F.; Liang, Z.; Liu, J.; Sun, J.; Hu, X.; Zhao, M.; Liu, J.; Bai, R.; Kim, D.; Sun, X.; Hyeon, T.; Ling, D. Dynamically Reversible Iron Oxide Nanoparticle Assemblies for Targeted Amplification of T_1-Weighted Magnetic Resonance Imaging of Tumors. *Nano Lett.* **2019**, 19 (7), 4213-4220.

(16) Li, X.; Lu, S. Y.; Xiong, Z. G.; Hu, Y.; Ma, D.; Lou, W. Q.; Peng, C.; Shen, M. W.; Shi, X. Y. Light-Addressable Nanoclusters of Ultrasmall Iron Oxide Nanoparticles for Enhanced and Dynamic Magnetic Resonance Imaging of Arthritis. *Adv. Sci.* **2019**, 6 (19), 1901800.

(17) Lu, J. X.; Sun, J. H.; Li, F. Y.; Wang, J.; Liu, J. N.; Kim, D.; Fan, C. H.; Hyeon, T.; Ling, D. S. Highly Sensitive Diagnosis of Small Hepatocellular Carcinoma Using pH-Responsive Iron Oxide Nanocluster Assemblies. *J. Am. Chem. Soc.* **2018**, 140 (32), 10071-10074.

(18) Kim, B. H.; Lee, N.; Kim, H.; An, K.; Park, Y. I.; Choi, Y.; Shin, K.; Lee, Y.; Kwon, S. G.; Na, H. B.; Park, J. G.; Ahn, T. Y.; Kim, Y. W.; Moon, W. K.; Choi, S. H.; Hyeon, T. Large-Scale Synthesis of Uniform and Extremely Small-Sized Iron Oxide Nanoparticles for High-Resolution T_1 Magnetic Resonance Imaging Contrast Agents. *J. Am. Chem. Soc.* **2011**, 133 (32), 12624-12631.

(19) Cao, Y.; He, Y. L.; Mao, Z.; Kuang, Y.; Liu, M.; Zhang, Y.; Pei, R. J. Synergistic Regulation of Longitudinal and Transverse Relaxivity of Extremely Small Iron Oxide Nanoparticles (ESIONPs) Using pH-Responsive Nanoassemblies. *Nanoscale* **2020**, 12 (33), 17502-17516.

(20) Wang, L.; Huang, J.; Chen, H.; Wu, H.; Xu, Y.; Li, Y.; Yi, H.; Wang, Y. A.; Yang, L.; Mao, H. Exerting Enhanced Permeability and Retention Effect Driven Delivery by Ultrafine Iron Oxide Nanoparticles with T_1-T_2 Switchable Magnetic Resonance Imaging Contrast. *ACS Nano* **2017**, 11 (5), 4582-4592.

(21) Zhou, H.; Tang, J.; Li, J.; Li, W.; Liu, Y.; Chen, C. In vivo Aggregation-Induced Transition Between T_1 and T_2 Relaxations of Magnetic Ultra-Small Iron Oxide Nanoparticles in Tumor Microenvironment. *Nanoscale* **2017**, 9 (9), 3040-3050.

(22) Wang, C. B.; Yan, C. L.; An, L.; Zhao, H. F.; Song, S. L.; Yang, S. P. Fe_3O_4 Assembly for Tumor Accurate Diagnosis by Endogenous GSH Responsive T_2/T_1 Magnetic Relaxation Conversion. *J. Mater. Chem. B*, **2021**, 9 (37), 7734-7740.

(23) Villaraza, A. J. L.; Bumb, A.; Brechbiel, M. W. Macromolecules, Dendrimers, and Nanomaterials in Magnetic Resonance Imaging: The Interplay between Size, Function, and Pharmacokinetics. *Chem. Rev.* **2010**, 110 (5), 2921-2959.

(24) Jia, L.; Li X.; Liu, H.; Xia J. D.; Shi X. Y.; Shen M. W. Ultrasound-Enhanced Precision Tumor Theranostics using Cell Membrane-Coated and pH-Responsive Nanoclusters Assembled from Ultrasmall Iron Oxide Nanoparticles. *Nano Today* **2021**, 36, 10102.

(25) Ma D.; Shi M. H.; Li X.; Zhang J. L.; Fan Y.; Sun K.; Jiang T. T.; Peng C.; Shi

X. Y. Redox-Sensitive Clustered Ultrasmall Iron Oxide Nanoparticles for Switchable T_2/T_1-Weighted Magnetic Resonance Imaging Applications. *Bioconjugate Chem.* **2020**, 31, 352−359.

(26) Kalyane, D.; Raval, N.; Maheshwari, R.; Tambe, V.; Kalia, K.; Tekade, R. K. Employment of Enhanced Permeability and Retention Effect (EPR): Nanoparticle-Based Precision Tools for Targeting of Therapeutic and Diagnostic Agent in Cancer. *Mater. Sci. Eng. C* **2019**, 98, 1252-1276.

(27) He, Y. L.; Cao, Y.; Mao, Z.; Zhou, Y. X.; Zhang, Y.; Pei, R. J. Redox-Triggered Aggregation of ESIONPs with Switchable T_1 to T_2 Contrast Effect for T_2-Weighted Magnetic Resonance Imaging. *J. Mater. Chem. B* **2021**, 9 (7), 1821-1832.

(28) He, Y. L.; Mao, Z.; Zhang, Y.; Lv, H. Y.; Yan, J. C.; Cao, Y.; Pei, R. J. Tumor Acid Microenvironment-Triggered Self-Assembly of ESIONPs for T_1/T_2 Switchable Magnetic Resonance Imaging. *ACS Appl. Bio Mater.* **2020**, 3 (11), 7752-7761.

(29) Zhou, H. G.; Guo, M. Y.; Li, J. Y.; Qin, F. L.; Wang, Y. Q.; Liu, T.; Liu, J.; Sabet, Z. F.; Wang, Y. L.; Liu, Y.; Huo, Q.; Chen, C. Y. Hypoxia-Triggered Self-Assembly of Ultrasmall Iron Oxide Nanoparticles to Amplify the Imaging Signal of a Tumor. *J. Am. Chem. Soc.* **2021**, 143, 1846−1853.

(30) Kataoka, K.; Harada, A.; Nagasaki, Y. Block Copolymer Micelles for Drug Delivery: Design, Characterization and Biological Significance. *Adv. Drug Delivery Rev.* **2012**, 64, 37-48.

(31) Wei, X. L.; Luo, Q.; Sun, L.; Li, X.; Zhu, H. Y.; Guan, P. J.; Wu, M.; Luo, K.; Gong, Q. Y. Enzyme- and pH-Sensitive Branched Polymer-Doxorubicin Conjugate-

Based Nanoscale Drug Delivery System for Cancer Therapy. *ACS Appl. Mater. Inter.* **2016**, 8 (18), 11765-11778.

(32) Zhu, C.; Zheng, M.; Meng, F.; Mickler, F. M.; Ruthardt, N.; Zhu, X.; Zhong, Z. Reversibly Shielded DNA Polyplexes Based on Bioreducible PDMAEMA-SS-PEG-SS-PDMAEMA Triblock Copolymers Mediate Markedly Enhanced Nonviral Gene Transfection. *Biomacromolecules* **2012**, 13 (3), 769-778.

(33) Gao, G. H.; Im, G. H.; Kim, M. S.; Lee, J. W.; Yang, J.; Jeon, H.; Lee, J. H.; Lee, D. S. Magnetite-Nanoparticle-Encapsulated pH-Responsive Polymeric Micelle as An MRI Probe for Detecting Acidic Pathologic Areas. *Small* **2010**, 6 (11), 1201-1204.

(34) Mo, Z. M.; Li, Q. T.; Zhao, K.; Xu, Q.; Hu, H.; Chen, X.; Luo, Y. X.; Chi, B.; Liu, L. P.; Fang, X. F.; Liao, G. F.; Xu, Z. S.; Wang, J.; Yang, S. L. A Nano architectonic Approach Enables Triple Modal Synergistic Therapies to Enhance Antitumor Effects. *ACS Appl. Mater. Interfaces* **2022**, 14 (8), 10001–10014.

(35) Liao, G. F.; He, F.; Li, Q.; Zhong, L.; Zhao, R. Z.; Che, H. N.; Gao, H. Y.; Fang, B. Z. Emerging Graphitic Carbon Nitride-based Materials for Biomedical Applications. *Prog. Mater. Sci.* **2020**, 112, 100666.

(36) Qin, Z. Z.; Qiu, M. J.; Zhang, Q. Y.; Yang S. L.; Liao, G. F.; Xiong, Z. F.; Xu, Z. S. Development of Copper Vacancy Defects in a Silver-doped CuS Nanoplatform for High-Efficiency Photothermal–Chemodynamic Synergistic Antitumor Therapy. *J. Mater. Chem. B* **2021**, 9, 8882-8896.

(37) Zou, Y. B.; Sun, F.; Liu, C. M.; Yu, C. H.; Zhang, M. J.; He, Q. Y.; Xiong, Y. X.; Xu, Z. S.; Yang, S. L.; Liao, G. F. A Novel Nanotheranostic Agent for Dual-Mode

Imaging-Guided Cancer Therapy based on Europium Complexes-Grafted-Oxidative Dopamine. *Chem. Eng. J.* **2019**, 357, 237–247.

(38) Ge, Z.; Liu, S. Functional Block Copolymer Assemblies Responsive to Tumor and Intracellular Microenvironments for Site-Specific Drug Delivery and Enhanced Imaging Performance. *Chem. Soc. Rev.* **2013**, 42 (17), 7289-325.

(39) Vila-Caballer, M.; Codolo, G.; Munari, F.; Malfanti, A.; Fassan, M.; Rugge, M.; Balasso, A.; de Bernard, M.; Salmaso, S. A pH-Sensitive Stearoyl-PEG-poly(methacryloyl sulfadimethoxine)-Decorated Liposome System for Protein Delivery: An Application for Bladder Cancer Treatment. *J. Controlled Release* **2016**, 238, 31-42.

(40) Abel, B. A.; Sims, M. B.; McCormick, C. L. Tunable pH- and CO_2- Responsive Sulfonamide-Containing Polymers by RAFT Polymerization. *Macromolecules* **2015**, 48 (16), 5487-5495.

(41) Hu, J.; Miura, S.; Na, K.; Bae, Y. H. pH-Responsive and Charge Shielded Cationic Micelle of Poly(L-histidine)-block-Short Branched PEI for Acidic Cancer Treatment. *J. Controlled Release* **2013**, 172 (1), 69-76.

(42) Baek, S.; Kim, D.; Jeon, S. L.; Seo, J. Preparation and Characterization of pH-Responsive Poly(N,N-Dimethyl Acrylamide-co-Methacryloyl Sulfadimethoxine) Hydrogels for Application as Food Freshness Indicators. *React. Funct. Polym.* **2017**, 120, 57-65.

(43) Cyphert, E. L.; von Recum, H. A.; Yamato, M.; Nakayama, M. Surface Sulfonamide Modification of Poly(N-Isopropylacrylamide)-Based Block Copolymer

Micelles to Alter pH and Temperature Responsive Properties for Controlled Intracellular Uptake. *J. Biomed. Mater. Res. A* **2018**, 106 (6), 1552-1560.

(44) Bertrand, A.; Stenzel, M.; Fleury, E.; Bernard, J. Host-Guest Driven Supramolecular Assembly of Reversible Comb-Shaped Polymers in Aqueous Solution. *Polym. Chem.* **2012**, 3 (2), 377-383.

(45) Zhang, Z. X.; Liu, K. L.; Li, J. Self-Assembly and Micellization of a Dual Thermoresponsive Supramolecular Pseudo-Block Copolymer. *Macromolecules* **2011**, 44 (5), 1182-1193.

(46) Paolino, M.; Ennen, F.; Lamponi, S.; Cernescu, M.; Voit, B.; Cappelli, A.; Appelhans, D.; Komber, H. Cyclodextrin-Adamantane Host-Guest Interactions on the Surface of Biocompatible Adamantyl-Modified Glycodendrimers. *Macromolecules* **2013**, 46 (9), 3215-3227.

(47) Hou, N.; Wang, R.; Geng, R.; Wang, F.; Jiao, T. F.; Zhang, L. X.; Zhou, J. X.; Bai, Z. H.; Peng, Q. M. Facile Preparation of Self-Assembled Hydrogels Constructed from Poly-Cyclodextrin and Poly-Adamantane as Highly Selective Adsorbents for Wastewater Treatment. *Soft Matter* **2019**, 15 (30), 6097-6106.

(48) Baek, S.; Kim, D.; Jeon, S. L.; Seo, J. Preparation and Characterization of pH-Responsive Poly(N,N-Dimethyl Acrylamide-co-Methacryloyl Sulfadimethoxine) Hydrogels for Application as Food Freshness Indicators. *React. Funct. Polym.* **2017**, 120, 57-65.

(49) Liu, Y. J.; Yang, Z.; Huang, X. L.; Yu, G. C.; Wang, S.; Zhou, Z. J.; Shen, Z. Y.; Fan, W. P.; Liu, Y.; Davisson, M.; Kalish, H.; Niu, G.; Nie, Z. H.; Chen, X. Y.

Glutathione-Responsive Self-Assembled Magnetic Gold Nanowreath for Enhanced Tumor Imaging and Imaging-Guided Photothermal Therapy. *ACS Nano* **2018**, 12 (8), 8129-8137.

(50) Lym, J. S.; Nguyen, Q. V.; Ahn, D. W.; Huynh, C. T.; Jae, H. J.; Kim, Y. I.; Lee, D. S. Sulfamethazine-based pH-Sensitive Hydrogels with Potential Application for Transcatheter Arterial Chemoembolization Therapy. *Acta Biomater.* **2016**, 41, 253-263.

(51) Guillet-Nicolas, R.; Bridot, J. L.; Seo, Y. B.; Fortin, M. A.; Kleitz, F. Enhanced Relaxometric Properties of MRI "Positive" Contrast Agents Confined in Three-Dimensional Cubic Mesoporous Silica Nanoparticles. *Adv. Funct. Mater.* **2011**, 21, 4653–4662.

(52) Neves, H. R.; Bini, r. a.; Barbosa, J. H. O.; Salmon, C. E. G.; Varanda, L. C. Dextran-Coated Antiferromagnetic MnO Nanoparticles for a T_1-MRI Contrast Agent with High Colloidal Stability. *Part. Part. Syst. Charact.* **201**6, 33, 167–176.

(53) Zhou, Z. X.; Han, Z.; Lu, Z. R. A Targeted Nanoglobular Contrast Agent from Host-Guest Self-Assembly for MR Cancer Molecular Imaging. *Biomaterials* **2016**, 85, 168-179.

(54) Vuong, Q. L.; Gossuin, Y.; Gillis, P.; Delangre, S. New Simulation Approach using Classical Formalism to Water Nuclear Magnetic Relaxation Dispersions in Presence of Superparamagnetic Particles used as MRI Contrast Agents. *J. Chem. Phys.* **2012**, 137, 114505.

(55) Vuong, Q. L.; Berret, J.; Fresnais, J.; Gossuin, Y. ; Sandre, Olivier. A Universal Scaling Law to Predict the Efficiency of Magnetic Nanoparticles as MRI T_2-Contrast

Agents. *Adv. Healthc. Mater.* **2012**, 1, 502-512.

(56) Arami, H.; Khandhar, A.; Liggitt, D.; Krishnan, K. M. In Vivo Delivery, Pharmacokinetics, Biodistribution and Toxicity of Iron Oxide Nanoparticles. *Chem. Soc. Rev.* **2015**, 44, 8576-8607.

(57) Kang, S. I.; Bae, Y. H. pH-Induced Solubility Transition of Sulfonamide-Based Polymers. *J. Controlled Release* **2002**, 80 (1-3), 145-155.

(58) Kang, S. I.; Bae, Y. H. pH-Induced volume-phase transition of hydrogels containing sulfonamide side group by reversible crystal formation. *Macromolecules* **2001**, 34 (23), 8173-8178.